Journal of Quantitative Spectroscopy & Radiative Transfer 180 (2016) 84–91

Contents lists available at ScienceDirect

Journal of Quantitative Spectroscopy & Radiative Transfer

journal homepage: www.elsevier.com/locate/jqsrt

A light-scattering study of Al_2O_3 abrasives of various grit sizes

Yuli W. Heinson, Amitabha Chakrabarti, Christopher M. Sorensen *

Department of Physics, Kansas State University, Manhattan, KS 66506, USA

ARTICLE INFO

Article history:
Received 9 February 2016
Received in revised form
17 April 2016
Accepted 18 April 2016
Available online

Keywords:
Light scattering
Irregularly shaped particles
Phase function
Dust particles

ABSTRACT

We report light scattering phase function measurements for irregularly shaped Al_2O_3 abrasive powders of various grit sizes. Q-space analysis is applied to the angular scattering to reveal a forward scattering regime, Guinier regime, power law regime with quantifiable exponents, and an enhanced backscattering regime. The exponents of the power laws for Al_2O_3 abrasives decrease with increasing internal coupling parameter ρ', which is in agreement with previous observations for other irregular particles. Unlike other dust particles previously studied showing single power laws under Q-space analysis, the largest three abrasives, for which $\rho' \gtrsim 100$, showed a kink in the power law, which is possibly due to the higher degree of symmetry for the abrasives than for all the particles studied previously. Direct comparison of the 1200, 1000, and 800 grit abrasive scattering to scattering by corresponding spheres shows that the scatterings approximately coincide at the spherical particle $qR \simeq \rho'$ crossover point. Furthermore, the scattering at the maximum $qR = 2kR$ by the irregularly shaped abrasives is close to the geometric centers of the glories of the spheres.

1. Introduction

Light scattering from spherical particles has been well studied and understood [1,2]; however, there is no complete description and understanding of light scattering by irregularly shaped particles. Much work including both experiment and theory has been conducted to study irregularly shaped particles [3–18]. However, few studies have changed relevant parameters in a systematic way which could lead to the uncovering of patterns. We chose to do light scattering phase function measurements from irregularly shaped Al_2O_3 abrasives due to their selectable sizes that allows for systematic variation of the size.

In this paper we describe experimental phase function measurements – scattered intensity as a function of angle – of Al_2O_3 abrasives and analyze the data with Q-space analysis. In Q-space analysis [19–21], the scattered intensity is plotted vs. the magnitude of the scattering wave vector q, which has the unit of inverse length, or the dimensionless qR, where R is a radial dimension, on a log–log scale. The magnitude of the scattering wave vector is derived as [22]

$$q = 2k \sin\left(\frac{\theta}{2}\right) \tag{1}$$

where $k = 2\pi/\lambda$ with λ the wave length and θ is the scattering angle. Unlike the conventional analysis (scattered intensity vs. θ) which yields nondescript, indistinguishable curves, Q-space analysis uncovers a pattern of features common to all shapes. The common pattern consists of a constant forward scattering lobe at small q, then with increasing q, a crossover, Guinier regime near $q \approx R^{-1}$, a power law regime with quantifiable exponents, and finally an enhanced backscattering regime [23]. The power law exponents decrease with increasing internal coupling

* Corresponding author.
E-mail address: sor@phys.ksu.edu (C.M. Sorensen).

http://dx.doi.org/10.1016/j.jqsrt.2016.04.017
0022-4073/

parameter ρ'. The internal coupling parameter ρ' [24] is defined as

$$\rho' = 2kR\left|\frac{m^2-1}{m^2+2}\right| \quad (2)$$

where m is the refractive index.

We chose to study abrasive particles because they have irregular shapes, are readily available and can be obtained in a range of sizes as specified by the manufacturer. Because the abrasive action requires rolling between the two surfaces that are grinding, they have a roughly spherical overall shape, as opposed to particles with large aspect ratios such as flakes or needles. Thus we anticipate that scattering by abrasive particles might have some characteristics in common with scattering by spheres. Our analysis below will directly compare the scattering by the abrasives with scattering by spheres under the eye of Q-space analysis. Moreover, the comparison will pay attention to both the forward and backward scattering properties in light of the discussion above and the possible power law that might lie in between.

2. Experiment

A $\lambda/4$ wave plate, after a 532 nm vertically polarized laser, with fast axis 45° from vertical was used to produce circularly polarized incident light (the same as unpolarized light to the detector). Our light scattering apparatus detects light scattered at 31 angles from 0.32° to 157° simultaneously. The forward scattering detection contains 16 angles from 0.32° to 9.9° and is based on a design by Ferri [25]. For the side scattering, a custom elliptical mirror (Optiforms) collects light at 15 angles from 15.3° to 157°. The detail of our light scattering apparatus is described in [26]. Similar as [26], a power meter was used to verify the experiment was under the single scattering limit by following the method described in [27].

We used a dust generator to aerosolize the abrasives [26]. The dust generator had a three inch in diameter and three inch tall cylindrical chamber into which the dust was loaded. The bottom of the chamber had a stir bar which spun at 200 revolutions per minute. Simultaneously, oxygen blew in from the bottom of the chamber. The outgoing aerosolized dust particles were directed to the scattering volume by vinyl tubing. We measured the phase function of 6 different grits of white Al_2O_3 abrasive powders from Panadyne Abrasives. For each measurement, 10 g of grit sample was loaded inside the dust generator chamber. Al_2O_3 is birefringent but the two refractive indices – 1.760 and 1.768 [28] – are very close to each other. Although they slightly change with wavelength, we treated the refractive index as 1.76 which would not significantly affect ρ'. The grit numbers and the average sizes in diameters of the abrasives were 1200 grit (3 μm), 1000 grit (4.5 μm), 800 grit (6.5 μm), 600 grit (9.3 μm), 400 grit (17.3 μm), and 320 grit (29.2 μm) as given by the manufacturer. The average sizes were determined by the openings of the screen through which the abrasives passed.

3. Al_2O_3 abrasives scattering results

We performed Q-space analysis on the angular scattering by the Al_2O_3 abrasives as shown from Figs. 1–6. The figures also contain corresponding optical microscope images. Each image has a 10 μm scale bar in the lower left and a scale bar in the upper right indicating the diameter given by the manufacturer for comparison to the image. The scattered intensity with arbitrary unit (a.u.) is plotted vs. $q(\mathrm{cm}^{-1})$ on a double logarithmic plot; this is Q-space analysis. For the smaller sizes, grits 1200, 1000, and 800 (note that the larger the grit number, the finer the powder), Q-space analysis reveals an indication of a constant forward scattering lobe at smallest q followed by, with increasing q, a Guinier regime, a power law regime and an enhanced backscattering regime. The power law exponents are labeled in each graph. For the larger sizes, grits 600, 400 and 320, the forward scattering and Guinier regimes could not be seen since the large size requires angles smaller than our minimum angle of 0.32°. Also, for the larger grits, a new feature appears starting perhaps with 800 grit and then growing with increasing size: a kink near $q \simeq 2 \times 10^4\ \mathrm{cm}^{-1}$. This kink perturbs the power law functionality.

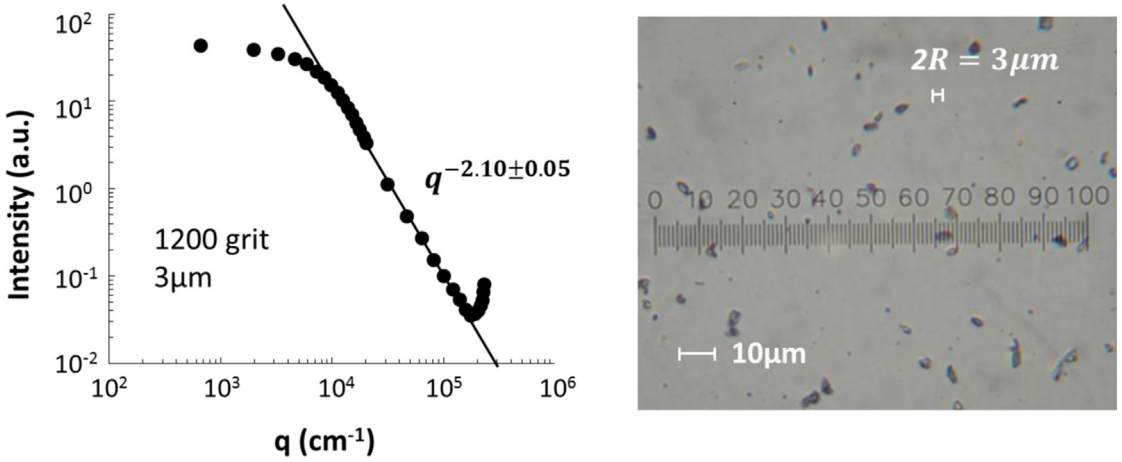

Fig. 1. Q-space analysis of scattering by 1200 grit Al_2O_3 abrasives and the corresponding image under an optical compound microscope.

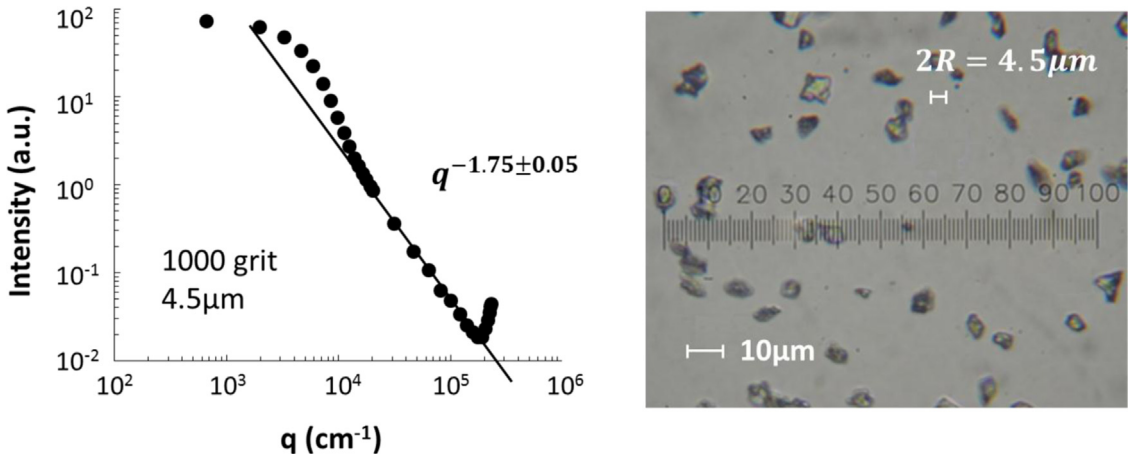

Fig. 2. Q-space analysis of scattering by 1000 grit Al_2O_3 abrasives and the corresponding image under an optical compound microscope.

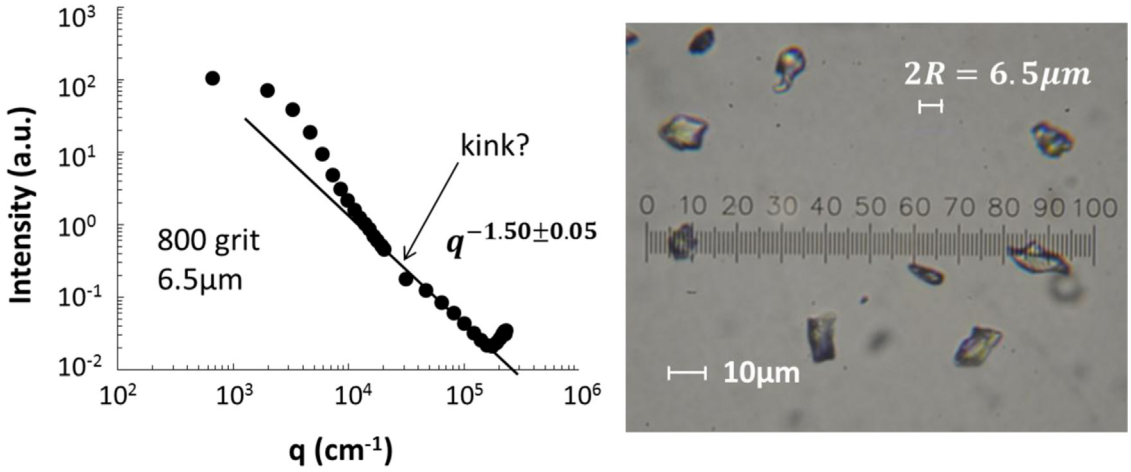

Fig. 3. Q-space analysis of scattering by 800 grit Al_2O_3 abrasives and the corresponding image under an optical compound microscope.

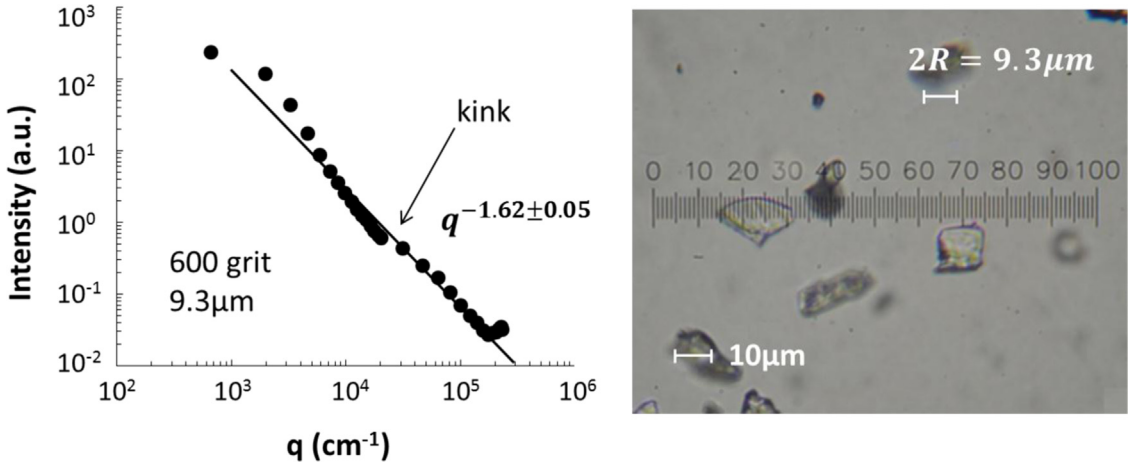

Fig. 4. Q-space analysis of scattering by 600 grit Al_2O_3 abrasives and the corresponding image under an optical compound microscope.

We have verified by calibrating the forward and side detectors to each other that the kink is not due to the misalignment or malfunction of our setup. This is substantiated by the fact that the kink does not exist for small abrasives and starts to develop with increasing sizes. Thus we are confident that the kink is an experimental fact.

As stated above, the size labeled in each figure is the average size of each abrasive sample given by the

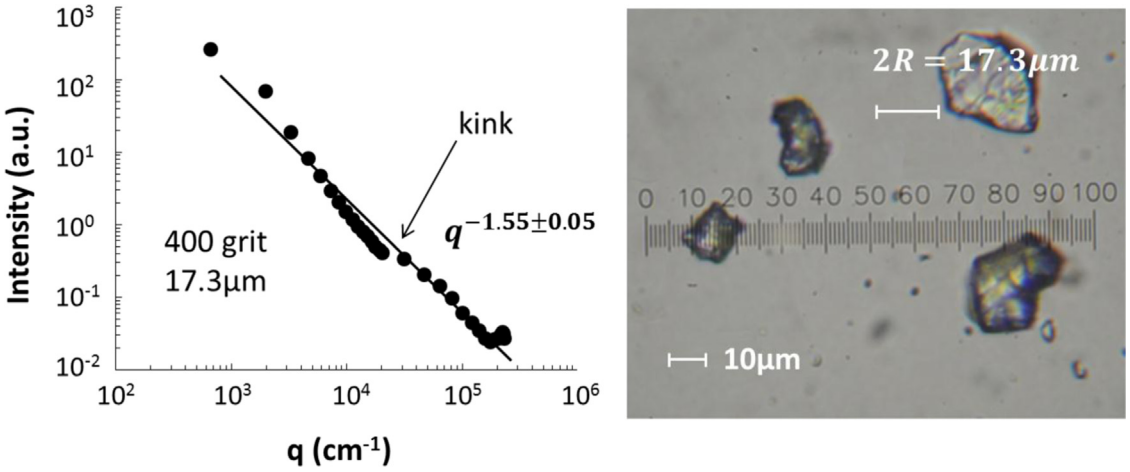

Fig. 5. Q-space analysis of scattering by 400 grit Al_2O_3 abrasives and the corresponding image under an optical compound microscope.

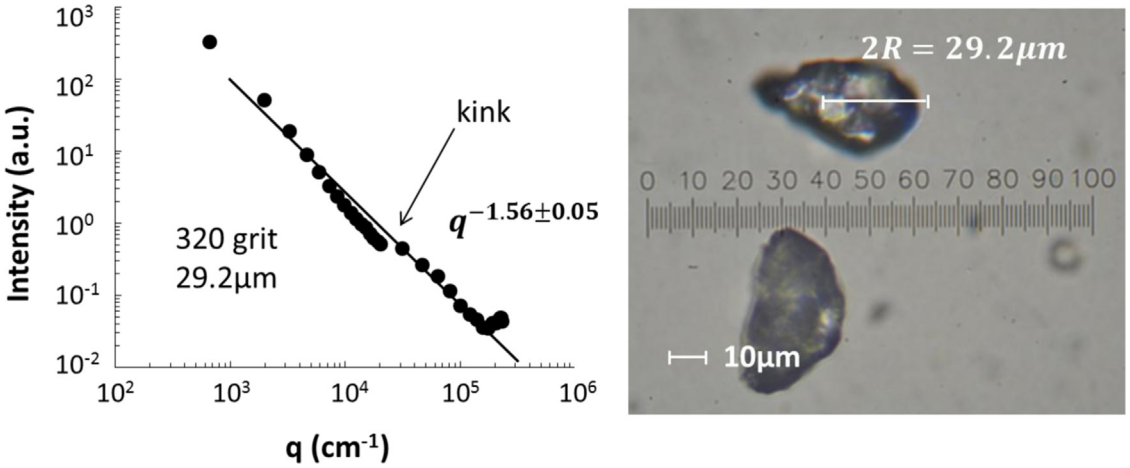

Fig. 6. Q-space analysis of scattering by 320 grit Al_2O_3 abrasives and the corresponding image under an optical compound microscope.

manufacture. However, light scattering tends to see the bigger particles of an ensemble of particles because bigger particles scattering more light. Hence, we need to determine the sizes from light scattering. Since the abrasives have irregular shapes, it is hard to define the sizes. However Guinier analysis of light scattering can yield the radius of gyration R_g which is exactly definable for any shape as

$$R_g^2 = \int_0^R r^2 \rho(\vec{r}) d^3 r / \int_0^R \rho(\vec{r}) d^3 r \tag{3}$$

where $\rho\left(\vec{r}\right)$ is the mass density at position $\vec{r}$ of an abrasive particle. In the limit $\rho' \to 0$ and when $qR_g < 1$, the Guinier equation [29] describes the forward scattering as

$$I(0)/I(q) = 1 + \frac{q^2 R_g^2}{3} \tag{4}$$

When $\rho' > 1$, the Guinier equation form still holds but the radius of gyration inferred from Eq. (4) is not the true radius of gyration [30]. For spheres when $\rho' > 30$, the ratio of the true to measured radii of gyrations is about 0.85($\pm$ 10%). Since a study similar to [30] has not been performed for non-spherical particles, and since the abrasive powders have a roughly spherical shape in some manner, we will apply this correction to the R_g we determine from a Guinier analysis of our abrasive light scattering.

The Guinier analysis [29] to determine the light scattering radius of gyration is shown in Fig. 7. Note the paucity of data in the Guinier regime which warns us not to expect great accuracy. We could only apply Guinier analysis to the 1200, 1000 and 800 grits which have relatively small sizes to ensure $qR_g < 1$. The 1200 grit has several points for the Guinier analysis. From the slope the radius of gyration of 1200 grit is 2.4 μm. For 1000 and 800 grits, the data are more limited. We put two boundary slopes for each set of data. The fit lines (solid lines) with smaller slopes only include two data points when $qR_g < 1$, where the Guinier analysis is, in principle, applicable; the fit lines (dashed lines) with larger slopes are the fits for all three data points in each data set. According to the fit line slopes, the ranges of the radii of gyration are between 3.7 μm and 3.9 μm for grit 1000 and between 6.4 μm and 6.9 μm for grit 800. From Guinier analysis, the measured radii of gyration of the 1000 and 800 grits were 3.8 $\pm$ 0.1 μm and 6.6 $\pm$ 0.3 μm. Given the uncertainties of radii of gyration of 1000 and 800 grits, the radius of the gyration of grit 1200 is 2.4 $\pm$ 0.1 μm. After the factor of 0.85 correction, the true radii of gyration were

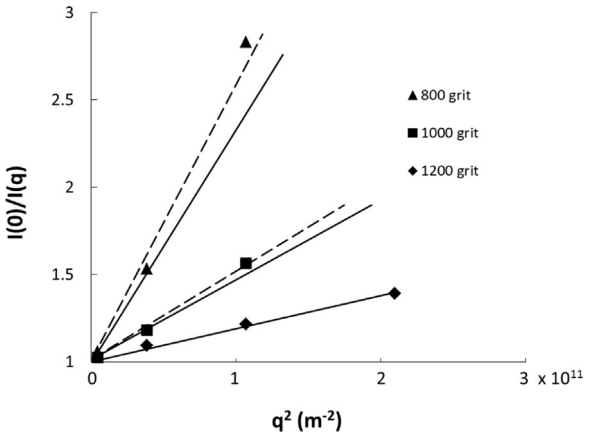

Fig. 7. Guinier analysis on Al_2O_3 abrasives of 1200, 1000, and 800 grit. The 1200 grit has several points for the Guinier analysis which indicates the radius of gyration is 2.4 μm. The data for 1000 and 800 grits are limited. The solid fit lines with smaller slopes only include two data points when $qR_g < 1$; the dashed fit lines with larger slopes are the fits for all three data points in each data set. According to the fit line slopes, the ranges of the radii of gyration are between 3.7 μm and 3.9 μm for grit 1000 and between 6.4 μm and 6.9 μm for grit 800.

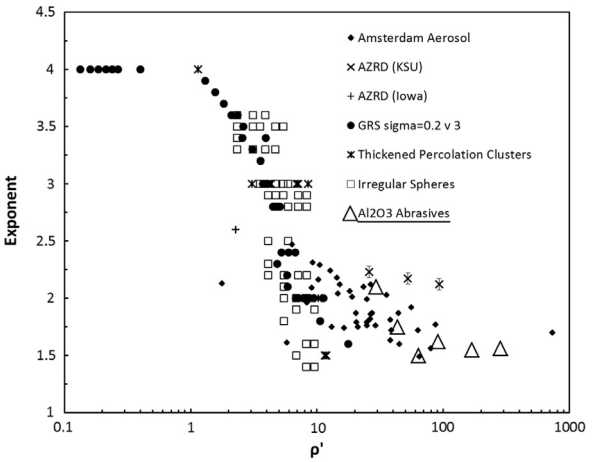

Fig. 8. Empirical correlation of Q-space power law exponents with the internal coupling parameter ρ' for a wide range of irregularly shaped particles [23]. The exponents for the Al_2O_3 abrasives shown as open triangles fit well to the quasi-universal behavior.

2.0 μm, 3.2 μm, and 5.6 μm, respectively, without considering the uncertainties. Mathematically, R_g is the root mean square radius which is smaller than the visible perimeter. The exact relation between R_g and the visible perimeter depends on the particle shape. Since we do not know the exact shape, we again make an approximation based on spheres where $R_g = \sqrt{3/5}R$. Therefore, the optical perimeter radii of the 1200, 1000, and 800 grits were 2.6 μm, 4.2 μm, and 7.2 μm, respectively; the optical perimeter diameters were 5.2 μm, 8.4 μm, and 14.4 μm, respectively. They are bigger than the sizes labeled in Figs. 1–3. Again, we have to consider the fact that light scattering tends to see the bigger particles of an ensemble of particles. The manufacturer claimed the average sizes of 1200, 1000, and 800 grits were 3 μm, 4.5 μm, and 6.5 μm correspondingly. However, the light scattering determined particle sizes were 5.2 μm, 8.4 μm, and 14.4 μm correspondingly which were twice as big as the sizes given by the manufacturer. Therefore, we made an assumption that the light scattering determined sizes for grit 600, 400, and 320 would be twice as big as the sizes given by the manufacturer as well. Unfortunately, we could not determine the light scattering determined sizes due to the request of smaller angle detection for grit 600, 400, and 320. When we calculated ρ's for the abrasives, we used the sizes twice as big as the ones given by the manufacturer.

4. Discussion

4.1. Power law exponent

In our recent, comprehensive work to study light scattering by irregularly shaped particles [23], we found that every particle type studied showed a uniform power law. Now, to the contrary, the three largest grits studied here show a kink in the power law. We will address this kink below when we compare abrasive scattering to spherical particle scattering. That previous work also showed that the power law exponents had a quasi-universal behavior with respect to the internal coupling parameter ρ'. In Fig. 8 we include the exponents for the grits, notwithstanding the kink, along with all the other exponents determined in that work (Fig. 8 is a reproduction of Fig. 9 from [23] with the six grits included). This demonstrates that the power law exponents from the grits follow the overall trend discovered in [23]. Note that the three largest grits, which showed the kink, are in a regime of $\rho' \gtrsim 100$ which was not explored in our previous work, save for the point at $\rho' \simeq 730$, the data for which did display a uniform power law.

4.2. Comparison between spheres and Al_2O_3 abrasives

In this section we make a comparison between the scattering from the irregularly shaped abrasives and perfect spheres with a polydisperse size distribution, using the perceptive eye of Q-space analysis. The comparison is semi-quantitative at best, but we believe it has value and points the way for future research. We compare grits and spheres of the same size and refractive index, hence with the same ρ'. Only the three smallest grits have well defined forward scattering and Guinier regimes to match to the same regimes for the spherical particles. To achieve the match we generated Mie solutions using Philip Laven MiePlot [31] to find a sphere radius that fit best to the abrasives Guinier regime for each grit. This was done under the condition of a spherical particle size distribution width of 1.2, which is used to eliminate the Mie scattering ripples.

Fig. 9(a)–(c) shows the comparisons between the spheres shown as dashed lines and the abrasives data shown as solid circles, where the scattered intensity (normalized at $qR \ll 1$) is plotted vs. qR. In Fig. 9 the abrasives scattering and the Mie scattering are forced to fit to each other in the Guinier regime so that we could see how they compare at large qR.

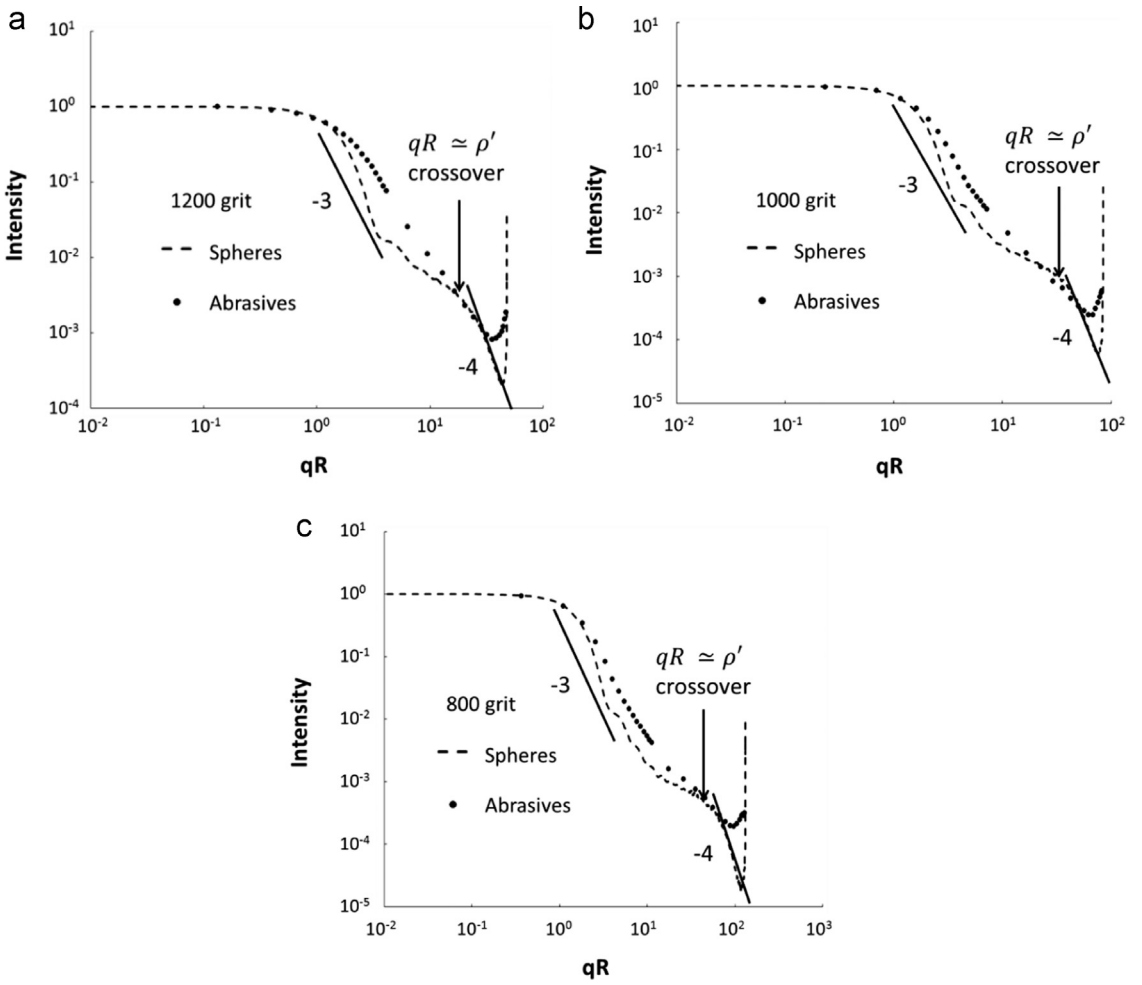

Fig. 9. Comparisons between scattering by spheres and the 1200, 1000, and 800 grit abrasives. The scattered intensity (normalized at $qR \ll 1$) is plotted vs. qR for each grit. Spheres and abrasives were forced to fit in the Guinier, $qR \ll 1$, range. Also indicated are the $qR \simeq \rho'$ crossover points for the sphere scattering.

The Q-space functionalities for spheres is as follows [24]: when $\rho' < 1$ (the Rayleigh–Debye–Gans (RDG) limit) a $(qR)^{-4}$ functionality follows the Guinier regime. With increasing ρ', a $(qR)^{-2}$ functionality appears after Guinier regime and then this falls back to a $(qR)^{-4}$ functionality when $qR \gtrsim \rho'$. As ρ' becomes larger, the $(qR)^{-2}$ functionality breaks into a $(qR)^{-3}$ regime followed by a relatively flat regime which then crosses over to a $(qR)^{-4}$ functionality when $qR \gtrsim \rho'$. We will call this the "$qR \simeq \rho'$ crossover". These functionalities are apparent in Fig. 9.

The comparison of the abrasive scattering to the spherical particle scattering in Fig. 9 uncovers some interesting features. At the $qR \simeq \rho'$ crossover, the scattering of the abrasives roughly touches the scattering due to the spheres. The end points of the scattering, i.e. the scattering at the maximum $qR = 2kR$, by the irregularly shaped abrasives are close to the geometric centers of the glories of the spheres. Along with these features, the rough $(qR)^{-3}$ immediately after the Guinier regime and the $(qR)^{-4}$ functionality for $qR \gtrsim \rho'$ are lost. One could say that the "roughening" of the spherical shape into that of the abrasives smoothed the intensity versus qR plot to leave a Guinier hump plus a single power law that is anchored by the Guinier regime and the $qR \simeq \rho'$ crossover. The same comparison was made in [32] between Gaussian Random Spheres (GRSs) and spheres to find the same result for the ending points, especially for large ρ'. Unfortunately, we cannot make direct comparison between GRSs and our abrasives because the smallest ρ' for our Al_2O_3 abrasives is larger than any GRS that we can currently solve for using computational techniques.

For the other three abrasives, 600, 400, and 320 grits, because the Guinier regime was not in the detectable range, we could not make direct comparisons to spheres. For spheres, the $(qR)^{-3}$ regime is a consequence of the crossover of the three dimensional spherical particle scattering to two-dimensional, Fraunhofer diffraction [33] which must occur when the sphere becomes very large and refractive. We expect a similar 3d to 2d crossover would occur for any shape at large enough ρ'. However, the regime before the kink for the abrasives does not show a $(qR)^{-3}$ functionality. The kink that occurs in the scattering for these three grits

developed with increasing size, thus it must be related to size. Note that Fig. 8 shows that these three grits are in a regime of large ρ' that was not covered in the previous work (save for the point at $\rho' = 730$ which was definitely a power law). Obviously this large ρ' region needs further study. If large ρ' is not the cause of the kink, we speculate that it could be due to the higher degree of symmetry for the abrasives than for all the particles studied previously.

5. Conclusions

We have measured the scattered light intensity for six different sizes of Al_2O_3 grits over a wide range of scattering angles starting at 0.32°. Q-space analysis of the scattering reveals a forward scattering regime at small q, followed by a crossover, Guinier regime near $q \approx R^{-1}$, a power law regime with quantifiable exponents, and an enhanced backscattering regime. The power law exponents decease with increasing internal coupling parameter ρ', which fits well to our previously observed quasi-universal behavior of the power law exponents with respect to ρ' for irregularly shaped particles. However, unlike that previous work, the largest three abrasive, for which $\rho' \gtrsim 100$, showed a kink in the power law. We directly compared the scattering of 1200, 1000, and 800 grit abrasives with corresponding spheres by finding the best fit in Guinier regime. At large qR, the scattering of the abrasives approximately coincides with that of the spheres at the $qR \simeq \rho'$ crossover point of the scattering from spheres, and the abrasive scattering follows a power law after the Guinier regime whereas the spherical particle scattering is much more complex. The scattering at the maximum $qR = 2kR$ by the irregularly shaped abrasives is close to the geometric centers of the glories of the spheres.

Finally, it is interesting to ponder why Q-space analysis uncovers features not seen with conventional plotting versus the scattering angle θ. The most important feature is that q has units of inverse length, and thus inverse q has units of length; it is the resolution length scale of the scattering experiment. Thus at small enough q, the resolution scale q^{-1} is larger than the size of the particle and so the scattering cannot resolve the particle thus shape is not a factor. Given this perspective, one can realize that a change in q will not change the scattering so long as q^{-1} is greater than the size. Continuing to larger q, as q^{-1} passes through the particle size, functionality must begin and that is the Guinier regime. Thereafter, the particle is well resolved by the scattering as a two dimensional object, regardless of shape, with two dimensional diffraction which has a q^{-3} Porod regime. This was approximately, but not completely obtained, for the particles here. At yet larger q, the scattering resolution becomes sharp enough to see the true three dimensional nature of the particle which yields a q^{-4} Porod regime. Finally, at the largest q, enhanced backscattering occurs even for non-spherical particles for reasons we do not know. These concepts for Q-space analysis can be found in more detail in Ref. [34].

Acknowledgments

The authors wish to thank Tim Sobering, Russell Taylor, and David Huddleston for the detectors electronic design. We are grateful to Russ Reynolds for his help on building and modifying our research instrumentation. This work is supported by National Science Foundation under Grant no. AGM 1261651 and U.S. Army Research Laboratory under Grant no. W911NF-14-1-0352.

References

[1] van de Hulst HC. Light scattering by small particles. Reprint edition. New York: Dover Publications; 1981.
[2] Bohren CF, Huffman DR. Absorption and Scattering of Light by Small Particles. New York: Wiley-VCH; 1998.
[3] Munoz O, Volten H, de Haan JF, Vassen W, Hovenier JW. Experimental determination of scattering matrices of olivine and Allende meteorite particles. Astron Astrophys 2000;360:777–88.
[4] Munoz O, Volten H, de Haan JF, Vassen W, Hovenier JW. Experimental determination of scattering matrices of randomly oriented fly ash and clay particles at 442 and 633 nm. J Geophys Res – Atmos 2001;106:22833–44.
[5] Munoz O, Volten H, de Haan JF, Vassen W, Hovenier JW. Experimental determination of the phase function and degree of linear polarization of El Chichon and Pinatubo volcanic ashes. J Geophys Res – Atmos 2002;107:4174.
[6] Munoz O, Volten H, Hovenier JW, Veihelmann B, van der Zande WJ, Waters L, et al. Scattering matrices of volcanic ash particles of Mount St. Helens, Redoubt, and Mount Spurr Volcanoes. J Geophys Res – Atmos 2004;109:D16201.
[7] Munoz O, Volten H, Hovenier JW, Min M, Shkuratov YG, Jalava JP, et al. Experimental and computational study of light scattering by irregular particles with extreme refractive indices: hematite and rutile. Astron Astrophys 2006;446:525–35.
[8] Munoz O, Volten H, Hovenier JW, Nousiainen T, Muinonen K, Guirado D, et al. Scattering matrix of large Saharan dust particles: experiments and computations. J Geophys Res – Atmos 2007;112:D13215.
[9] Munoz O, Moreno F, Guirado D, Dabrowska DD, Volten H, Hovenier JW. The Amsterdam–Granada light scattering database. J Quant Spectrosc Radiat Transf 2012;113:565–74.
[10] Volten H, Munoz O, Rol E, de Haan JF, Vassen W, Hovenier JW, et al. Scattering matrices of mineral aerosol particles at 441.6 nm and 632.8 nm. J Geophys Res – Atmos 2001;106:17375–401.
[11] Volten H, Muñoz O, Brucato JR, Hovenier JW, Colangeli L, Waters LBFM, et al. Scattering matrices and reflectance spectra of forsterite particles with different size distributions. J Quant Spectrosc Radiat Transf 2006;100:429–36.
[12] Laan EC, Volten H, Stam DM, Munoz O, Hovenier JW, Roush TL. Scattering matrices and expansion coefficients of martian analogue palagonite particles. Icarus 2009;199:219–30.
[13] Dubovik O, Sinyuk A, Lapyonok T, Holben BN, Mishchenko M, Yang P, et al. Application of spheroid models to account for aerosol particle nonsphericity in remote sensing of desert dust. J Geophys Res – Atmos 2006;111:D11208.
[14] Kalashnikova OV, Sokolik IN. Modeling the radiative properties of nonspherical soil-derived mineral aerosols. J Quant Spectrosc Radiat Transf 2004;87:137–66.
[15] Muinonen K. Introducing the Gaussian shape hypothesis for asteroids and comets. Astron Astrophys 1998;332:1087–98.
[16] Muinonen K, Lagerros JSV. Inversion of shape statistics for small solar system bodies. Astron Astrophys 1998;333:753–61.
[17] Nousiainen T, Munoz O, Lindqvist H, Mauno P, Videen G. Light scattering by large Saharan dust particles: comparison of modeling and experimental data for two samples. J Quant Spectrosc Radiat Transf 2011;112:420–33.
[18] Nousiainen T, Lindqvist H, McFarquhar GM, Um J. Small irregular ice crystals in tropical cirrus. J Atmos Sci 2011;68:2614–27.
[19] Sorensen CM, Fischbach DJ. Patterns in Mie scattering. Opt Commun 2000;173:145–53.
[20] Berg MJ, Sorensen CM, Chakrabarti A. Patterns in Mie scattering: evolution when normalized by the Rayleigh cross section. Appl Opt 2005;44:7487–93.

[21] Sorensen CM. Q-space analysis of scattering by particles: a review. J Quant Spectrosc Radiat Transf 2013;131:3–12.
[22] Sorensen CM. Light scattering by fractal aggregates: a review. Aerosol Sci Technol 2001;35:648–87.
[23] Heinson YW, Maughan JB, Heinson WR, Chakrabarti A, Sorensen CM. Light scattering Q-space analysis of irregularly shaped particles. J Geophys Res – Atmos 2015. http://dx.doi.org/10.1002/2015JD024171.
[24] Heinson WR, Chakrabarti A, Sorensen CM. A new parameter to describe light scattering by an arbitrary sphere. Opt Commun 2015;356:612–5.
[25] Ferri F. Use of a charge coupled device camera for low-angle elastic light scattering. Rev Sci Instrum 1997;68:2265–74.
[26] Wang Y, Chakrabarti A, Sorensen CM. A light-scattering study of the scattering matrix elements of Arizona Road Dust. J Quant Spectrosc Radiat Transf 2015;163:72–9.
[27] Mokhtari T, Sorensen CM, Chakrabarti A. Multiple scattering effects on optical structure factor measurements. Appl Opt 2005;44:7858–61.
[28] Palik ED. In: Handbook of optical constants of solids II.New York: Academic Press; 1997.
[29] Guinier A, Fournet G, Yudowitch KL. In: Small-angle scattering of x-rays. 1st ed.New York: Wiley; 1955.
[30] Sorensen CM, Shi D. Guinier analysis for homogeneous dielectric spheres of arbitrary size. Opt Commun 2000;178:31–6.
[31] Laven P. Simulation of rainbows, coronas, and glories by use of Mie theory and the Debye series. J Quant Spectrosc Radiat Transf 2004;89:257–69.
[32] Maughan JB, Sorensen CM, Chakrabarti A. Q-space analysis of light scattering by Gaussian Random Spheres. J Quant Spectrosc Radiat Transf 2016;174:14–21.
[33] Hecht E. In: Optics.San Francisco: Addison-Wesley; 2002.
[34] Oh C, Sorensen CM. Scaling approach for the structure factor of a generalized system of scatterers. J Nanopart Res 1999;1:369–77.